

## 1.6 W high wall plug efficiency, continuous-wave room temperature quantum cascade laser emitting at 4.6 $\mu\text{m}$

A. Lyakh,<sup>1,a)</sup> C. Pflügl,<sup>2,b)</sup> L. Diehl,<sup>2</sup> Q. J. Wang,<sup>2</sup> Federico Capasso,<sup>2</sup> X. J. Wang,<sup>3</sup> J. Y. Fan,<sup>3</sup> T. Tanbun-Ek,<sup>3</sup> R. Maulini,<sup>1</sup> A. Tsekoun,<sup>1</sup> R. Go,<sup>1</sup> and C. Kumar N. Patel<sup>1,4,c)</sup>

<sup>1</sup>Pranalytica, Inc., 1101 Colorado Ave., Santa Monica, California 90401, USA

<sup>2</sup>School of Engineering and Applied Sciences, Harvard University, Cambridge, Massachusetts 02138, USA

<sup>3</sup>Adtech Optics, Inc., 18007 Cortney Court, City of Industry, California 91748, USA

<sup>4</sup>Department of Physics and Astronomy, University of California, Los Angeles, California 90095, USA

(Received 22 January 2008; accepted 25 February 2008; published online 20 March 2008)

A strain-balanced, InP-based quantum cascade laser structure designed for light emission at 4.6  $\mu\text{m}$  was grown by metal-organic chemical vapor deposition. A maximum total optical power of 1.6 W was obtained in continuous-wave mode at 300 K for uncoated devices processed in buried heterostructure geometry with stripe dimensions of 5 mm by 9.5  $\mu\text{m}$ . Corresponding maximum wall plug efficiency and threshold current density were measured to be 8.8% and 1.05 kA/cm<sup>2</sup>, respectively. Fully hermetically packaged laser of identical dimensions produced in excess of 1.5 W under the same conditions. © 2008 American Institute of Physics. [DOI: 10.1063/1.2899630]

Low atmospheric absorption in the wavelength range from 3 to 5  $\mu\text{m}$ , known as the first atmospheric window, lends itself to several important applications for high-power quantum cascade lasers (QCLs). Photon energy in this wavelength range ( $\sim 275$  meV for  $\lambda = 4.5$   $\mu\text{m}$ ) comprises a large fraction of the band offset of conventional lattice-matched AlInAs/InGaAs (520 meV). Therefore, highly strained InP-based material has been used for high-performance QCLs emitting at  $\lambda < 5.5$   $\mu\text{m}$ .<sup>1-5</sup> The introduction of strain leads to higher barriers and, as a consequence, reduced thermal escape of electrons from the lowest injector and the upper laser states into the continuum. Continuous-wave (cw) QCL operation,<sup>6</sup> required, for example, for photoacoustic spectroscopy,<sup>7</sup> has an impediment of strong laser active region self-heating compared to pulsed operation. Higher active region temperature is detrimental to laser performance as it leads to higher threshold current, lower slope efficiency, lower maximum optical power, and lower wallplug efficiency (WPE). Therefore, the active region needs to be designed to suppress the undesirable high temperature effects such as reduction of the injection efficiency and increase in the electron backfilling of the lower laser level. In addition, the waveguide design of QCLs meant to be operated in cw needs to be optimized for effective heat dissipation from the active region while maintaining very low optical losses and high mode confinement factor. In this manuscript, we present our work on such optimization of a strain-balanced AlInAs/InGaAs QCL structure.

The active region of our structure is based on highly strained (1%) In<sub>0.67</sub>Ga<sub>0.33</sub>As/Al<sub>0.64</sub>In<sub>0.36</sub>As quantum wells and barriers with strain compensation in each stage. The band offset, the effective mass and the non parabolicity coefficient for this material system were calculated according to Refs. 8 and 9 and slightly adjusted to obtain a good agreement between the results of our simulations and the experimental data obtained with several structures. The laser transition energy  $E_{43}$ , the laser transition matrix element  $z_{43}$ , and the upper laser level lifetime  $\tau_4$  were calculated to be

275 meV ( $\lambda = 4.5$   $\mu\text{m}$ ), 1.48 nm, and 1.77 ps, respectively (using level numbering convention in Ref. 6). To suppress parasitic carrier injection into a higher energy level 5 (that located in the active region above the upper laser level) at high active region temperatures, the energy spacing  $E_{54}$  was designed to be above 60 meV. In addition, to reduce electron thermal backfilling of the lower laser level 3 caused by long carrier extraction (tunneling) time from the lowest active region state 1,<sup>10</sup> the energy spacing  $E_{31}$  was designed to be approximately 100 meV. Similar to a traditional two-phonon resonance design,<sup>11</sup> the energy spacing  $E_{32}$  in our design was equal to the energy of the longitudinal optical phonon (34 meV). However, in contrast to a two-phonon design,  $E_{21}$  was designed to be approximately 70 meV. The phonon-limited lifetimes  $\tau_3$  and  $\tau_2$  were calculated to be 0.26 and 0.34 ps respectively, close to typical values for the two-phonon design. The large value of  $E_{21}$  did not lead to a longer electron lifetime  $\tau_2$  because our design had two, instead of one, closely spaced (18 meV) lowest active region states 1 and 1', both having large overlaps with state 2. The so-called voltage defect  $\Delta$ , defined as the energy spacing between the lower laser level and the lowest state of the following injector, was 138 meV, close to 150 meV typically used in QCL design. We believe that this small difference does not have a considerable impact on laser performance. However, further voltage defect reduction will lead to increased carrier back scattering for the lower laser level and, as a consequence, lower laser performance.

The optical waveguide was designed to have low optical losses  $\alpha_w$  and a large overlap factor of the optical mode with the gain medium. A buried heterostructure (BH) laser with a narrow width is the most effective way to achieve these goals and in addition to maximize the heat dissipation from the waveguide core.<sup>2,4,5</sup> Due to its high thermal conductivity, InP was chosen to form the cladding layers. In order to reduce  $\alpha$ , the doping was kept low ( $3 \times 10^{16}$  cm<sup>-3</sup>) in the portion of the cladding layers having a significant overlap with the optical mode. The rest of the waveguide structure essentially consists of relatively thick low doped ( $1 \times 10^{17}$  cm<sup>-3</sup>) InP layers and a highly doped ( $8 \times 10^{18}$  cm<sup>-3</sup>) plasmon layer which help decouple the optical mode from the lossy metal contact.

<sup>a)</sup>Electronic mail: alyakh@pranalytica.com.

<sup>b)</sup>Electronic mail: pflugl@seas.harvard.edu.

<sup>c)</sup>Electronic mail: patel@pranalytica.com.

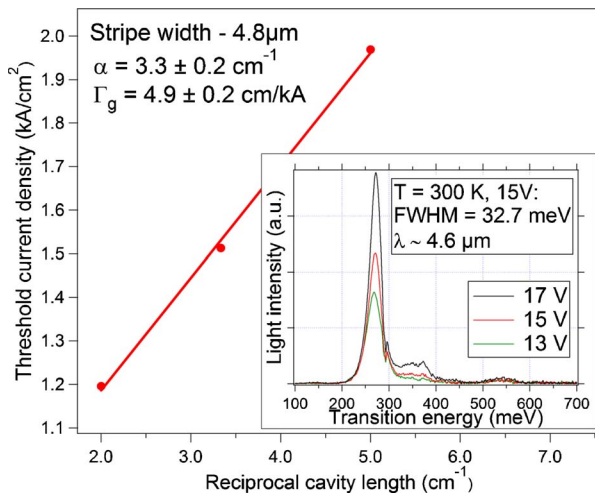


FIG. 1. (Color online) Pulsed threshold current density dependence on reciprocal cavity length for lasers with stripe width of  $4.8 \mu\text{m}$ . Waveguide optical loss  $\alpha_w$  and modal differential gain  $\Gamma g$  were found from the plot to be  $3.3 \text{ cm}^{-1}$  and  $4.9 \text{ cm/kA}$ , respectively. Inset: electroluminescence spectra of a mesa device fabricated from the wafer. Full width at half maximum (FWHM) was measured to be  $32.7 \text{ meV}$  at  $15 \text{ V}$ .

The doping of each of the layers composing the waveguide was optimized to limit not only  $\alpha_w$  but also the series resistance of the device. The efficient heat dissipation of narrow BH devices allows a thick active region to be utilized. In our structure, we increased the number of periods from the usual value of 30 to 40. This led to an increase in confinement factor of the  $\text{TM}_{00}$  mode in a  $4.8 \mu\text{m}$  wide BH device from 63% to 72% and to a proportional increase in slope efficiency of the optical power versus current characteristic.

The QC laser material discussed in this work was grown by low pressure metal-organic chemical vapor deposition (MOCVD), as described in Ref. 12. The epitaxial layer sequence starting from the InP substrate ( $3 \times 10^{18} \text{ cm}^{-3}$ ) was as follows:  $1.5 \mu\text{m}$  InP cladding layer ( $1 \times 10^{17} \text{ cm}^{-3}$ ),  $1.5 \mu\text{m}$  InP cladding layer ( $3 \times 10^{16} \text{ cm}^{-3}$ ),  $1.8 \mu\text{m}$  active region consisting of the 40-stage AlInAs-InGaAs QC strain-balanced structure,  $1.5 \mu\text{m}$  InP cladding layer ( $3 \times 10^{16} \text{ cm}^{-3}$ ),  $1.5 \mu\text{m}$  InP cladding layer ( $1 \times 10^{17} \text{ cm}^{-3}$ ),  $1.0 \mu\text{m}$  InP plasmon layer ( $8 \times 10^{18} \text{ cm}^{-3}$ ), and a  $0.2 \mu\text{m}$  heavily doped InGaAs contact layer.

Initially, part of the wafer was processed into mesa devices. The inset of Fig. 1 shows their electroluminescence spectra obtained at room temperature and at different voltages. Spectrum measured at  $15 \text{ V}$  (within the operational voltage range) was centered at an energy corresponding to  $\sim 4.6 \mu\text{m}$ , very close to the designed value of  $4.5 \mu\text{m}$ . The residual discrepancy is due, in part, to uncertainties in the parameters (band offset, effective mass, nonparabolicity coefficient) used in our model, as well as to the nonideal shape of the barrier interface and to the effects of high strain in the heterostructure layers. The full width at half maximum (FWHM) of this spectrum was  $32.7 \text{ meV}$ .

The wafer was then processed into BH laser chips. The devices were subsequently cleaved and mounted episcide down on aluminum nitride (AlN) submounts, as described in Ref. 13 using AuSn solder for long term robustness. In addition to its excellent thermal conduction properties, AlN has been shown to ensure long QCL device lifetime and high reliability.

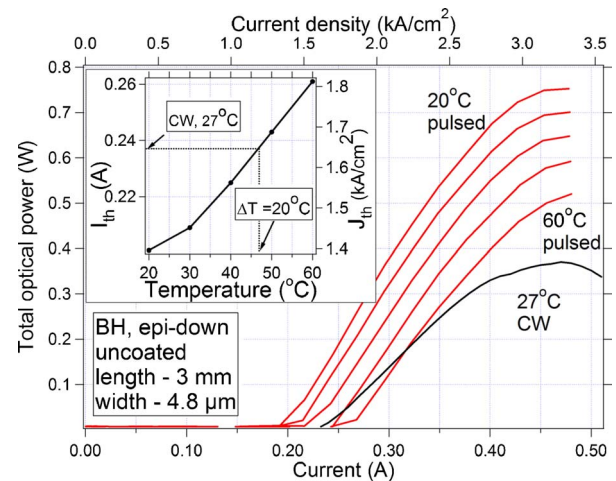


FIG. 2. (Color online) Light vs current curves of a  $3 \text{ mm}$  long, uncoated device with stripe width of  $4.8 \mu\text{m}$  in pulsed (red,  $250 \text{ ns}$ ,  $10 \text{ kHz}$ ) and cw (black) modes. The inset shows threshold current density dependence on temperature in pulsed mode, yielding active region temperature rise in cw mode at threshold of  $20 \text{ K}$ .

Figure 1 shows the pulsed threshold current density dependence on the reciprocal cavity length for lasers with stripe width equal to  $4.8 \mu\text{m}$ . The waveguide optical loss  $\alpha_w$  was found from the plot to be  $3.3 \text{ cm}^{-1}$ , which is comparable with previously reported data for QCLs emitting close to this wavelength.<sup>4</sup> Our simulations show that only 10% of the experimental value found for  $\alpha_w$  originates from the waveguide itself, and the rest comes from intersubband absorption in the heterostructure.

Figure 2 shows the light versus current ( $LI$ ) characteristics of a  $3 \text{ mm}$  long device of  $4.8 \mu\text{m}$  stripe width in both pulsed ( $250 \text{ ns}$ ,  $10 \text{ kHz}$ ) and cw modes. The inset shows the variation of pulsed threshold current density with device temperature. This allowed us to extract the value of active region temperature rise at threshold in cw regime at  $300 \text{ K}$ , measured to be  $20 \text{ K}$ , and corresponding to thermal conductance  $G_{\text{th}} = 1169 \text{ W}/(\text{K cm}^2)$ . Pulsed WPE for this device at  $30^\circ \text{C}$  was measured to be approximately 10%, with cw WPE being half as much. In order to reduce the threshold current density and improve output power and WPE, we reduced the contribution of mirror losses to the total optical losses by fabricating devices with longer cavity lengths.

cw power and voltage versus current characteristics ( $LIV$ ) for a  $5 \text{ mm}$  long uncoated laser with  $9.5 \mu\text{m}$  stripe width are shown in Fig. 3 along with WPE. The maximum total optical power (including both facets) was measured to be  $1.6 \text{ W}$  at  $300 \text{ K}$ , the highest value reported so far for a single QCL in cw mode at room temperature. After correction for the measurement setup wiring resistance equal to  $0.26 \Omega$ , maximum WPE was found to be 8.8%. In addition, the cw threshold current density was measured to be  $1.05 \text{ kA/cm}^2$ . Slope efficiency of  $2.7 \text{ W/A}$  for the  $5 \text{ mm}$  long laser was substantially higher than  $\sim 2.1 \text{ W/A}$  measured in cw mode for the  $3 \text{ mm}$  device at the same temperature. This is in contrast to the fact that the slope efficiency in pulsed mode, proportional to the ratio of the mirror losses to the total losses, is expected to be higher for the shorter device. We explain this by detrimental temperature effects on QCL performance in cw mode operation. Lower mirror losses lead to lower threshold current density for longer devices and lower active region temperature at threshold. As a

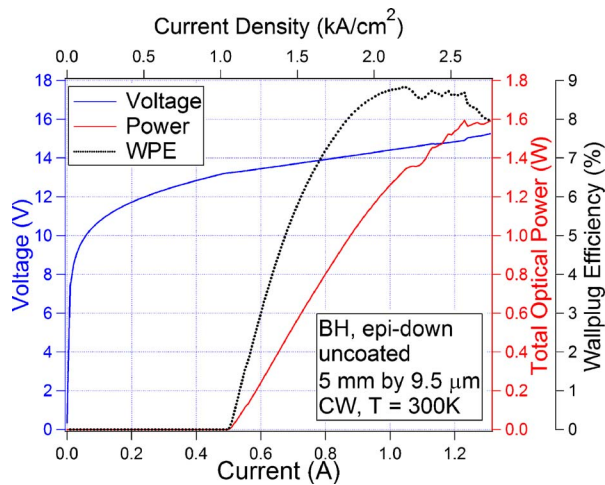


FIG. 3. (Color online) cw *LIV* and WPE measured at 300 K for a 5 mm long, uncoated laser chip with stripe width of  $9.5 \mu\text{m}$ .

consequence, undesirable active region heating effects, such as reduction in the injection efficiency and upper laser level electron lifetime, are decreased in this case.

The same device was then assembled in a fully hermetic, butterfly-style package. The package incorporates a thermoelectric cooler (TEC) and custom collimating lenses. Light is coupled out via antireflection coated hermetic windows. We theoretically estimated and experimentally measured optical collection efficiency of this package to exceed 90%. The package is designed to operate on an air-cooled heat sink. Figure 4 shows the photograph of the package with top lid removed for clarity. Figure 5 shows *LIV* and WPE for the packaged device. Laser temperature was maintained by the TEC at 300 K. Maximum total optical power from the device incorporated in the hermetic package was measured to be 1.5 W and corresponding WPE approached 8.2% without correcting for package optical collection efficiency.

In conclusion, we have presented the design and characterization for an MOCVD-grown QCL structure optimized for cw, room temperature operation, emitting at  $4.6 \mu\text{m}$ . Our BH QCLs emitted very high maximum optical power (1.6 W) with low threshold current density and high WPE (8.8%). Fully hermetically packaged in a butterfly-style package, these devices produced 1.5 W of useful output at 300 K laser temperature. Since the TEC integrated into our hermetic package allows a reduction of chip operating temperature, even higher output power and WPE is possible. Operating a  $7 \mu\text{m}$  stripe, 3 mm long high reflection coated QCL in the hermetically sealed package at chip temperature

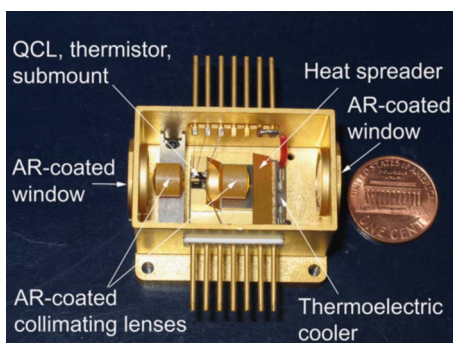


FIG. 4. (Color online) Photograph of our hermetic butterfly-style package with top lid removed for clarity.

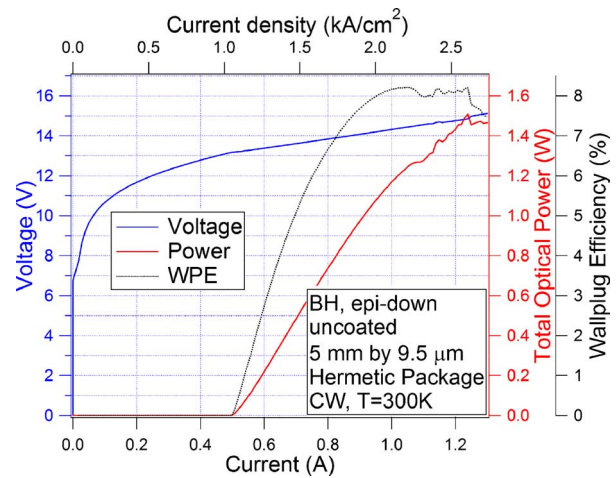


FIG. 5. (Color online) cw *LIV* and WPE measured at laser temperature of 300 K for a 5 mm long, uncoated laser chip with stripe width of  $9.5 \mu\text{m}$  in a hermetic butterfly-style package. Data shown are not corrected for package optical collection efficiency.

of 270 K (package temperature of 302 K), we have achieved WPE of nearly 12% (without correcting for package optical collection efficiency). Present level of performance and device integration already permits incorporation of these lasers into practical applications, such as photoacoustic spectroscopy, free space optical communications, and infrared countermeasures where high-power midinfrared lasers are required. User friendly, fully packaged devices of this performance level pave the way to a broad adoption of QCL technology by the end users.

This work was supported in part through a DARPA Contract No. W911QX-07-C-0041 (approved for public release, Distribution Unlimited). The work at Harvard University was performed in part at the Center for Nanoscale Systems (CNS), a member of the National Nanotechnology Infrastructure Network (NNIN), which was supported by the National Science Foundation under NSF Award No. ECS-0335765. A. Lyakh and C. Pflügl equally contributed to this work.

- <sup>1</sup>A. Evans, J. Yu, S. Slivken, and M. Razeghi, *Appl. Phys. Lett.* **85**, 2166 (2004).
- <sup>2</sup>L. Diehl, D. Bour, S. Corzine, J. Zhu, G. Höfler, B. Lee, C. Wang, M. Troccoli, and F. Capasso, *Appl. Phys. Lett.* **88**, 041102 (2006).
- <sup>3</sup>A. Evans, J. Nguyen, S. Slivken, J. Yu, S. Darvish, and M. Razeghi, *Appl. Phys. Lett.* **88**, 051105 (2006).
- <sup>4</sup>L. Diehl, D. Bour, S. Corzine, J. Zhu, G. Höfler, M. Lončar, M. Troccoli, and F. Capasso, *Appl. Phys. Lett.* **89**, 081101 (2006).
- <sup>5</sup>A. Evans, S. Darvish, S. Slivken, J. Nguyen, Y. Bai, and M. Razeghi, *Appl. Phys. Lett.* **91**, 071101 (2007).
- <sup>6</sup>M. Beck, D. Hofstetter, T. Aellen, J. Faist, U. Oesterle, M. Ilegems, E. Gini, and H. Melchior, *Science* **295**, 301 (2002).
- <sup>7</sup>M. Pushkarsky, I. Dunayevskiy, M. Prasanna, A. Tsekoun, and C. K. N. Patel, *Proc. Natl. Acad. Sci. U.S.A.* **103**, 19630 (2006).
- <sup>8</sup>C. G. Van de Walle, *Phys. Rev. B* **39**, 1871 (1989).
- <sup>9</sup>M. Sugarawa, N. Okazaki, T. Fujii, and S. Yamazaki, *Phys. Rev. B* **48**, 8002 (1993).
- <sup>10</sup>J. Faist, D. Hofstetter, M. Beck, T. Aellen, M. Rochat, and S. Blaser, *IEEE J. Quantum Electron.* **38**, 533 (2002).
- <sup>11</sup>D. Hofstetter, M. Beck, T. Aellen, and J. Faist, *Appl. Phys. Lett.* **78**, 396 (2001).
- <sup>12</sup>X. Wang, J. Fan, T. Tanbun-Ek, and F.-S. Choa, *Appl. Phys. Lett.* **90**, 211103 (2007).
- <sup>13</sup>A. Tsekoun, R. Go, M. Pushkarsky, M. Razeghi, and C. K. N. Patel, *Proc. Natl. Acad. Sci. U.S.A.* **103**, 4831 (2006).